HHS Public Access

Author manuscript

Biomacromolecules. Author manuscript; available in PMC 2024 March 12.

Published in final edited form as:

Biomacromolecules. 2023 January 09; 24(1): 413–425. doi:10.1021/acs.biomac.2c01218.

Synthesis, Characterization, and Digital Light Processing of a Hydrolytically Degradable Hyaluronic Acid Hydrogel

Jonathan H. Galarraga[1,‡], **Abhishek P. Dhand**[1,‡], **Bruce P. Enzmann III**[1], **Jason A. Burdick**[1,2,*]

[1]Department of Bioengineering, School of Engineering and Applied Sciences, University of Pennsylvania, Philadelphia, PA 19104, USA

[2]BioFrontiers Institute and Department of Chemical and Biological Engineering, University of Colorado, Boulder, CO 80303, USA

Abstract

Numerous chemical modifications of hyaluronic acid (HA) have been explored for the formation of degradable hydrogels that are suitable for a variety of biomedical applications, including biofabrication and drug delivery. Thiol-ene step-growth chemistry is of particular interest due to its lower oxygen sensitivity and ability to precisely tune mechanical properties. Here, we utilize an aqueous esterification route via reaction with carbic anhydride to synthesize norbornene-modified HA ($NorHA_{CA}$) that is amenable to thiol-ene crosslinking to form hydrolytically unstable networks. $NorHA_{CA}$ is first synthesized with varying degrees of modification (~15–100%) by adjusting the ratio of reactive carbic anhydride to HA. Thereafter, $NorHA_{CA}$ is reacted with dithiol crosslinker in the presence of visible light and photoinitiator to form hydrogels within tens of seconds. Unlike conventional NorHA, $NorHA_{CA}$ hydrogels are highly susceptible to hydrolytic degradation through enhanced ester hydrolysis. Both the mechanical properties and the degradation timescales of $NorHA_{CA}$ hydrogels are tuned via macromer concentration and/or the degree of modification. Moreover, the degradation behavior of $NorHA_{CA}$ hydrogels is validated through a statistical-co-kinetic model of ester hydrolysis. The rapid degradation of $NorHA_{CA}$ hydrogels can be adjusted by incorporating small amounts of slowly degrading NorHA macromer into the network. Further, $NorHA_{CA}$ hydrogels are implemented as digital light processing (DLP) resins to fabricate hydrolytically degradable scaffolds with complex, macroporous structures that can incorporate cell adhesive sites for cell attachment and proliferation after fabrication. Additionally, DLP bioprinting of $NorHA_{CA}$ hydrogels to form cell-laden constructs with

[*]**Corresponding Author** Jason A. Burdick (jason.burdick@colorado.edu).

[‡]These authors contributed equally to this work

Author Contributions

The manuscript was written through contributions of all authors. All authors have given approval to the final version of the manuscript.

Supporting Information (PDF)

Supplemental details regarding statistical-co-kinetic model of hydrogel degradation behavior

Figures S1 – S16; ^{1}H-NMR spectra, rheological and morphological characterization, polymer content of $NorHA_{CA}$ hydrogels over time, cumulative release of BSA from $NorHA_{CA}$ hydrogels, degradation of $NorHA_{CA}$ hydrogels in the presence of hyaluronidase, working curve and DLP print characterization, bMSC cell viability post-printing

Tables S1 – S2; Representative examples of previously reported 3D printed hydrolytically degradable hydrogels and theoretical degradation rate constants for various $NorHA_{CA}$ hydrogel formulations

high viability is demonstrated, making them useful for applications in tissue engineering and regenerative medicine.

Graphical Abstract

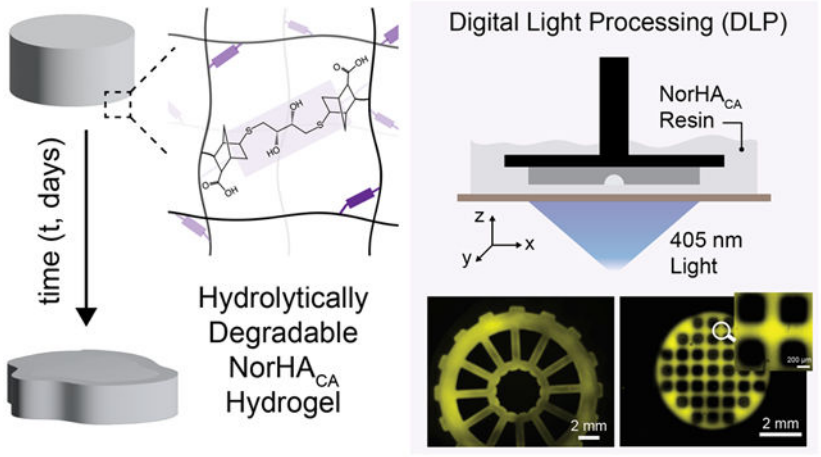

Keywords

hyaluronic acid; hydrolytic degradation; digital light processing; macroporous

1. INTRODUCTION

Hydrogels have gained significant attention in biomedical research, particularly due to their ability to recapitulate properties of native tissue and cellular microenvironments[1] and to encapsulate therapeutics for delivery to diseased tissues or to modulate the behavior of encapsulated cells.[2] Hydrogels with controlled and predictable degradation behaviors are especially desirable for biomedical applications. For example, degradable hydrogels have been employed as delivery vehicles in cell-based therapies for the repair of damaged tissues, as surgical adhesives, and as implants to recruit and stimulate endogenous cells in regenerative medicine.[3,4]

To control the degradation of hydrogels, the crosslinking chemistry employed and the extent of crosslinking may be varied.[4] As an example, physically crosslinked hydrogels erode through disruption of the intermolecular interactions involved in crosslinks (e.g., disruption of ionic bonds in Ca^{2+}-crosslinked alginate hydrogels in the presence of calcium chelating compounds).[5] In contrast, covalently crosslinked hydrogels are typically degraded by cleavage of the network backbone or crosslinks, with degradation induced through exposure to light,[6,7] enzyme activity,[8-11] environmental stimuli (pH,[12] temperature[13]), or hydrolysis.[14-16] Enzymatic degradation of hydrogels is highly dependent on the local environment since the local enzyme concentration and activity can appreciably influence degradation kinetics. Conversely, hydrolytically degradable hydrogels may be engineered with degradation timescales that are defined *a priori* by the network hydrophilicity, structure,

and crosslink density. Therefore, hydrolytically degradable hydrogels are of special interest in biomedical applications where precise degradation timescales are desired.

Hyaluronic acid (HA) is a naturally occurring glycosaminoglycan that is found in the extracellular matrix of many tissues and that has been used extensively in clinical products.[17] HA consists of alternating d-glucuronic acid and N-acetyl-d-glucosamine units and is rapidly turned over in the body via hyaluronidases.[18] HA macromers with hydrolytically sensitive functional groups have been previously synthesized for use as tissue engineering scaffolds, including with the incorporation of caprolactone or lactic acid units between the HA backbone and reactive groups (i.e., methacrylate).[19,20] However, these macromers are often crosslinked via free radical crosslinking. In contrast, macromers that undergo step-growth crosslinking (e.g., thiol-ene reaction) can offer more precise control over mechanical properties by simply altering the ratio of thiols to norbornenes;[21] however, there are few current options available towards this. Recently, polymer modifications been performed with carbic anhydride to functionalize norbornene groups for downstream thiol-ene crosslinking.[16,22-25] Modification with carbic anhydride results in the conjugation of norbornenes with an additional carboxylic acid group, which significantly increases the overall hydrophilicity of the pendant norbornene to accelerate the hydrolysis of ester bonds found between the norbornene and the macromer backbone.

In the context of this study, HA is modified with pendant norbornene groups via reaction with carbic anhydride ($NorHA_{CA}$) to form hydrolytically degradable step-growth hydrogels. Thorough experimental characterization of degradation and mechanics, as well as the implementation of a model to relate the stochastic degradation of $NorHA_{CA}$ crosslinks to macroscopic hydrogel properties over time, are undertaken to better understand $NorHA_{CA}$ hydrogels. Additionally, the fabrication of macroporous $NorHA_{CA}$ scaffolds is introduced via digital light processing (DLP) of these reactive resins. Despite significant recent advances in additive manufacturing, the 3D printing of hydrolytically degradable hydrogels with DLP remains limited and only a few examples exist (Table S1).

2. MATERIALS AND METHODS

2.1. Macromer synthesis and characterization:

All chemicals were obtained from Millipore-Sigma unless stated otherwise. Sodium hyaluronate (HA, average mol. wt. = 88 kDa, Lot #028842, ENG-00200) was obtained from Lifecore Biomedical (USA).

To synthesize norbornene-modified HA via reaction with carbic anhydride ($NorHA_{CA}$), HA (3.4 g) was first dissolved in deionized water (0.2 L) on ice at 0° C. Depending on the desired degree of modification, carbic anhydride (4.18 – 27.9 g, 20 equivalents) was then added to the solution and the pH was maintained at 8.5-9.5 throughout the 4-5 h reaction via dropwise addition of sodium hydroxide (1 N, NaOH), and then the reaction was continued overnight. In case of solid impurities or unreacted CA, the solution was centrifuged, and the supernatant was then transferred to dialysis tubing (Spectra Por, 6-8 kDa cutoff) and dialyzed against deionized water for 3 days, frozen at −80° C, and lyophilized. Dry polymer was stored under inert nitrogen at −20° C. To obtain $NorHA_{CA}$ with varying degrees of

modification, the amount of carbic anhydride was adjusted accordingly. To determine the degree of modification of HA, lyophilized macromer (10 mg) was dissolved in deuterium oxide (D_2O, 1 mL) and characterized using ^{1}H-NMR spectroscopy (Bruker Neo400 360 MHz) (Figure S1). Modification of HA with pendant norbornene groups was determined by integration of vinyl protons (2H, δ ~ 5.8 to 6.2 ppm) relative to the methyl group on HA (δ ~ 1.8 to 2.2 ppm, 3H). Additionally, the presence of peaks corresponding to norbornene functional groups (alkene and bridge protons) and absence of impurities was confirmed by comparing ^{1}H-NMR spectra of $NorHA_{CA}$ (product) with unmodified HA and CA (reactants) (Figure S2).

Norbornene-modified HA (NorHA) without the additional carboxylic acid group was synthesized as previously described via di-tert-butyl dicarbonate (Boc_2O) coupling of 5-norbornene-2-carboxylic acid to the pendant alcohols of HA.[21] First, HA was converted into its tetrabutylammonium salt form (HA-TBA) by mixing aqueous solution of HA (5 g) with Dowex 50Wx200 proton exchange resin (15 g) for 30 minutes, filtering the resin, and titrating the filtrate with tetrabutylammonium hydroxide (0.2 M) solution to a pH of 7.02–7.05. HA-TBA solution was then frozen and lyophilized. Next, HA-TBA (3.5 g) was dissolved in anhydrous dimethyl sulfoxide (DMSO, ~0.25 L) along with 5-norbornene-2-carboxylic acid (1.7 mL) and 4-(dimethylamino)pyridine (0.85 g) under inert nitrogen at 45° C. After complete dissolution, Boc_2O (0.6 mL) was added and the reaction was allowed to proceed for 20 h. Thereafter, the reaction was quenched with cold deionized water. The solution was then dialyzed for 14 days, frozen, lyophilized, and stored under nitrogen at −20 °C and characterized with ^{1}H-NMR to determine the extent of norbornene modification of HA. To determine zeta potential, all macromers (10 mg) were dissolved in ultrapure distilled water (1 mL) and measurements were obtained at 25 °C using disposable DTS1070 capillary cells on a Zetasizer Nano (Malvern Instruments).

2.2. Hydrogel Fabrication and Mechanical Testing:

$NorHA_{CA}$ or NorHA (1 – 5 wt.%) were dissolved in Dulbecco's (1×) phosphate buffered saline (PBS) along with photoinitiator (lithium phenyl-2,4,6-trimethylbenzoylphosphinate, LAP, 1.7 mM, Colorado Photopolymer Solutions, USA) and crosslinker (dithiothreitol, DTT, 2 – 48 mM, 1:1 thiol:norbornene ratio) to form precursor solutions. All precursor solutions were vortexed, cast into molds, and crosslinked in the presence of visible light (5 min, 10 mW cm^{-2}, Exfo Omnicure Vis S1000 lamp, 400-500 nm filter). Rheological characterization was performed on an AR2000 stress-controlled rheometer (TA Instruments) fitted with a 20 mm diameter parallel plate geometry and 100 μm gap. The gelation kinetics were obtained through time sweeps (0.5% strain, 1 Hz, time to gel point defined as the crossover between storage modulus, G', and loss modulus, G'') in the presence of visible light. Hydrogels were cast into 4.5 mm diameter cylindrical discs for compression testing (Q800 DMA, TA Instruments, 0.2 N min^{-1} force ramp). Compressive moduli were determined from the linear elastic region (10-20% strain) of the stress-strain curves.

2.3. Characterization of hydrogel degradation behavior:

Hydrogels (4.5 mm diameter discs) were immersed in PBS (1 mL) at 37° C until the complete degradation of the hydrogel (i.e., reverse gelation) was observed. Throughout the

incubation time course, the supernatant was collected periodically and replaced with fresh PBS. The supernatant was frozen at −80° C until analysis for uronic acid content. For NorHA hydrogel samples that did not undergo complete reverse gelation, hyaluronidase (750–3000 U mL^{-1}) was added to the solution to induce complete degradation on the last day of incubation (to identify the total amount of uronic acid incorporated and released within each respective hydrogel formulation). Uronic acid content was determined following a previously reported 96-well based protocol.[26] Briefly, supernatant samples for each time point (50 μL) were mixed with 25 mM sodium tetraborate in sulfuric acid (200 μL) and incubated at 100 °C for 10 min. After cooling to room temperature, 0.125% carbazole in ethanol (50 μL) was added to each sample well and heated at 100 °C for 10 min. The absorbance of samples was recorded at 550 nm on a Tecan Infinite M200 spectrometer, with a four-parameter sigmoidal regression used to fit generated standard curves (concentrations ranging from 0 – 1 mg mL^{-1} HA).

In addition to uronic acid release, the compressive moduli (described above) and the wet weight of the swollen gels were recorded at regular intervals. Day 0 refers to the timepoint at which compressive moduli and mass of the hydrogel were measured immediately after crosslinking. Mass swelling ratios (Q_m) were calculated as the ratio of the swollen gel mass (m_s) to that of dry polymer after lyophilization (m_d).[27] To characterize cumulative release of proteins, bovine serum albumin (BSA, 10 mg mL^{-1}) or lysozyme (5 mg mL^{-1}) were encapsulated within hydrogels incubated in PBS at 37 °C, and the supernatant was collected regularly. Protein release was detected over time using the Pierce™ BCA Protein Assay Kit (Thermo Fisher Scientific) in accordance with the manufacturer's protocol. Briefly, supernatant samples for each time point (25 μL) were mixed with working reagent (200 μL, 50:1 BCA Reagent A:B) in a 96-well plate and incubated at 37 °C for 30 min. After cooling to room temperature, sample absorbance was recorded at 562 nm on a Tecan Infinite M200 spectrometer, with a four-parameter sigmoidal regression used to fit generated standard curves with concentrations ranging between 0 – 2 mg mL^{-1} BSA.

2.4. Modeling of hydrogel degradation behavior:

A custom MATLAB script was developed using an object-oriented programming approach to simulate the random degradation of crosslinks within $NorHA_{CA}$ hydrogels. The model is based on a previously reported stochastic model that describes the hydrolysis of thiol-ene crosslinked dextran hydrogels.[28] Briefly, an array of crosslinkable 'nodes' was first constructed based on input macromer properties and hydrogel formulation, where each column (n) represents an individual polymer chain (n=1000 polymer chains simulated per each modeled network) and each row (m) corresponds to a discrete norbornene group attached to the polymer chain backbone, such that an index ($x_{n,m}$) was assigned to every norbornene actively forming a crosslink within the network. Model inputs included the macromer concentration, macromer molecular weight, repeat unit molecular weight, the degree of polymer chain backbone modification, and the hydrogel volume, all of which informed the total number of crosslinks incorporated into the simulated network. Within each simulated network, the number of degraded crosslinks was monitored as a function of time. As a result, the average number of active functional groups participating within crosslinks was determined and thereafter related to macroscopic hydrogel properties of

interest, including mass swelling ratios and compressive moduli. Please refer to Supporting Information for additional methods.

2.5. DLP-based 3D printing and patterning:

$NorHA_{CA}$ resin was composed of $NorHA_{CA}$ macromer (5 wt.%, 40% mod.), LAP (17 mM), DTT (24 mM) and tartrazine photoabsorber (1 mM). To identify the optimal printing conditions (i.e., to obtain a working curve), $NorHA_{CA}$ resins with different concentrations of incorporated tartrazine (0.5–1 mM) were exposed to a range of irradiation doses (varied exposure times, intensity = 15 mW cm^{-2}) and the thicknesses of the resultant crosslinked films were measured using calipers. 3D printing was then performed on a Lumen Alpha DLP bioprinter (Volumetric Inc., USA) as previously described.[29,30] Briefly, the resin was added into the vat, the build platform was lowered (30 mm min^{-1}) into the resin bath, and construct layers were then crosslinked sequentially with light exposure (6 s, 15 mW cm^{-2}, 100 μm step size). DLP-based 3D printing of a resin composed of mixed $NorHA_{CA}$ (4.5 wt.%, 40% mod.) and NorHA (0.5 wt.%, 30% mod.) was conducted in a similar manner with 6 s of light exposure for each layer, whereas 3 s of light exposure was chosen for NorHA (5 wt.%, 30% mod.) resin alone. Post-printing, printed hydrogel constructs were removed from the build platform, washed with PBS to remove excess or uncured resin, immersed in a PBS solution containing LAP (17 mM) and DTT (15 mM), and post-cured with visible light exposure (10 mW cm^{-2}, Exfo Omnicure Vis S1000 lamp, 400-500 nm filter, 5 min, with constructs flipped after 2.5 min of curing). CAD models were either designed in Fusion 360 (Autodesk, USA) or downloaded from online repositories (NIH 3D print exchange and MakerBot Thingiverse). For maskless patterning, pre-formed hydrogel films or 3D-printed hydrogels (with off-stoichiometric thiol-norbornene consumption) were soaked in 0.1 mM fluorescent thiol (GCDDD-Fluor; N-terminal fluorophore – 5-carboxyfluorescein, Genscript) solution for 30 minutes followed by light exposure (8 s, 15 mW cm^{-2}, 405 nm) on the DLP printer. Following light illumination, the hydrogels were washed, soaked in PBS overnight at 4 °C on a shaker to remove excess/unconjugated fluorescent thiol, and imaged on a confocal microscope.

2.6. Imaging and Visualization of Printed Constructs:

0.5 mg mL^{-1} of rhodamine-labeled dextran (500 kDa) or FITC-labeled dextran (2 MDa) was added to the hydrogel precursor before DLP-based 3D printing. Images of hydrogel constructs (in air) were then acquired with a Sony Alpha 7R3 camera. Macroscopic fluorescent images were acquired on a wide-field microscope (Axio Zoom V.16, Zeiss, Germany) and z-stack (5-20 μm step size) fluorescence scans were acquired on a confocal microscope (Leica SP5). Images were then pseudo-colored and brightness/contrast adjusted for 3D visualization using ImageJ (NIH).

2.7. Cell Culture, Seeding, Encapsulation and Visualization:

Bovine bone marrow-derived mesenchymal stromal cells (bMSCs) were isolated from a juvenile bovine knee joint (Research 87 Inc., USA) and used for all experiments. Cell culture media was comprised of high-glucose Dulbecco's modified Eagle's medium (DMEM, 1×) supplemented with 10% v/v fetal bovine serum and 1% v/v penicillin–streptomycin. For cell seeding experiments, hydrogel specimens were prepared (cast or

3D printed) as described earlier (with 2 mM thiolated RGD, GCGYGRGDSPG, Genscript), washed with PBS, and sterilized with germicidal UV lamp for 1 h. Cells (p1) were seeded (density: 7500 cells cm^{-2}) on hydrogels and cultured at 37 °C in a 5% CO_2 incubator for up to a week with media replaced every other day. Cells were fixed with neutral buffered formalin (10% v/v), permeabilized with Triton X-100 (0.1% v/v), and stained with fluorescein-conjugated phalloidin (1:500; Thermo Fisher Scientific) and Hoechst 33342 (1:1000; Thermo Fisher Scientific) to visualize F-actin and nuclei, respectively.

For cell encapsulation experiments, $NorHA_{CA}$ or NorHA macromers were sterilized under germicidal lamp for 1 h and then dissolved in a sterile solution of PBS, LAP (1.7 mM), DTT, and RGD (2 mM). Cells (p1-p2) were washed, trypsinized, mixed with precursor solution at a cell density of 5×10^6 cells mL^{-1} and cast into hydrogels with visible light exposure (3 min, 10 mW cm^{-2}, Exfo Omnicure Vis S1000 lamp, 400-500 nm filter). For bioprinting studies, $NorHA_{CA}$ precursor solution containing cells (density: 2×10^6 cells mL^{-1}) and photoabsorber (tartrazine, 1 mM) was dispensed onto a sterile vat and 3D printed as described earlier. Post-printing or casting, the hydrogels were washed thoroughly with warm cell-culture media and incubated (37 °C, 5% CO_2) for up to 7 days with media replaced every other day. To assess viability, cell-laden gels were incubated with calcein AM (2 μM) and ethidium homodimer-1 (4 μM) at 37 °C for 30 minutes following manufacturer's protocol (Live/Dead™ Cytotoxicity Kit, Thermo Fisher Scientific). Z-stack images were acquired on a Nikon Eclipse Ti2 with AXR scanner confocal microscope equipped with a 2× or 20× immersion objective lens. Cell number was calculated based on the total number of nuclei (binary mask, Otsu threshold) from maximum projection images analyzed on ImageJ (NIH). Cell viability was calculated as the number of live cells divided by the total number of cells within a single image maximum projection image. Images were pseudo-colored and brightness/contrast adjusted for 3D visualization.

2.8. Statistical Analysis:

All data are reported as mean ± standard deviation with $n \geq 3$. All statistics were conducted using Prism 9 (GraphPad Inc., USA). Comparisons between two experimental groups were performed using two-tailed t-tests ($\alpha = 0.05$, significance determined at $p < 0.05$) and comparisons between more than two groups were performed using a one-way analysis of variance (ANOVA) with post hoc Tukey's multiple comparison test.

3. RESULTS AND DISCUSSION

3.1. Fabrication and Characterization of $NorHA_{CA}$ Hydrogels.

HA is modified with norbornene functional groups via esterification with carbic anhydride (CA) to synthesize the macromer $NorHA_{CA}$. The esterification reaction occurs between the primary alcohol group on the HA backbone and anhydride, resulting in an additional carboxylic acid group on the conjugated, pendant norbornene moiety (Figure 1a). Contrary to traditional synthesis routes for NorHA, which require the formation of an intermediate HA-TBA salt and the use of organic solvents, this synthesis is a one-step reaction that proceeds under aqueous conditions, thereby reducing the total time required for macromer synthesis (Figure 1). Based on previous studies, we believe that the additional carboxylic

acid group incorporated with this synthesis approach increases the susceptibility of the ester group to hydrolysis.[16,31] Importantly, the degree of modification can be easily controlled by varying the molar ratio of CA to overall HA repeat units in the reaction, yielding $NorHA_{CA}$ macromers with ~15 to 100% degree of modification as verified through ^{1}H-NMR (Figures 1b, S1). The zeta potential of these synthesized $NorHA_{CA}$ macromers varies with degree of modification ranging from −38.6 ± 3.5 mV (15% mod.) to −52.4 ± 4.3 mV (100% mod.) (Figure S3). This decrease in charge with increase in the degree of modification is expected given the increase in the carboxylic acid group on norbornenes would increase the negative charge to $NorHA_{CA}$. Similar to traditional NorHA hydrogels, $NorHA_{CA}$ can be crosslinked into a covalent network via a thiol-ene step growth reaction in the presence of photoinitiator (lithium phenyl-2,4,6-trimethylbenzoylphosphinate, LAP), crosslinker (dithiothreitol, DTT), and visible light (400 – 500 nm) (Figure 1c).

We verify the thiol-ene crosslinking of $NorHA_{CA}$ hydrogels (1:1 stoichiometric ratio of thiol to norbornene) via oscillatory shear rheology with light exposure. Low viscosity $NorHA_{CA}$ precursor solution transitions into a crosslinked network (storage modulus, G' > loss modulus, G'') upon exposure to light within seconds or tens of seconds (Figure 2a-c). This is seen across all $NorHA_{CA}$ formulations independent of the macromer concentration (i.e., 1, 3, 5 wt.%) or the degree of norbornene modification (i.e., 15, 40, 100%). The storage and loss moduli of $NorHA_{CA}$ hydrogels generally increase with macromer concentration due to the associated increases in reactive norbornene concentration, resulting in storage moduli ranging from 0.18 ± 0.06 to 36.53 ± 4.62 kPa (Figure 2d,e, Figure S4). Similarly, this also results in faster photo-gelation kinetics, as evidenced by the decrease in time to gel point (characterized as the crossover between G' and G'') across macromer concentrations at a fixed degree of $NorHA_{CA}$ modification (Figure 2f). Overall, the time to gelation ranged from 11 to 28 seconds for the various formulations investigated.

Next, we characterize the hydrolytic stability of $NorHA_{CA}$ hydrogels incubated in phosphate buffered saline (PBS) at 37 °C. To investigate the degradation of $NorHA_{CA}$ hydrogels, we quantify the release of uronic acid from the hydrogel, as well as changes in the compressive modulus, mass swelling ratio, and polymer content over time (Figure 3, Figure S5). Rapid degradation is observed across all $NorHA_{CA}$ formulations, with reverse gelation occurring between 3 to 14 days. Consistent with the enhanced mechanical properties observed via rheological characterization (Figure 2), higher macromer concentrations (at a fixed degree of modification) or higher degrees of modification (at a fixed polymer concentration) result in $NorHA_{CA}$ hydrogels that remain for longer periods prior to degradation; this may be attributed to the corresponding increases in the network crosslinking densities within hydrogels. Further, it is important to note that at a fixed macromer concentration, an increase in the degree of modification results in a subsequent increase in the norbornene functional group concentration. At low macromer concentrations, network defects are more likely to arise for macromers with high degree of substitution than those with lower, resulting in comparable mechanical properties. Such network defects combined with the higher hydrophilicity likely contributes to faster degradation of $NorHA_{CA}$ (1 wt.%, 100% mod.) hydrogels as compared to $NorHA_{CA}$ (1 wt.%, 40% mod.).

Across all of the investigated hydrogel formulations, degradation is evidenced by gradual increases in uronic acid release and marked reductions in the compressive modulus over time. For instance, $NorHA_{CA}$ (5 wt.%, 40% mod.) hydrogels exhibit decreased compressive moduli from 74.2 ± 2.1 kPa to 1.2 ± 0.5 kPa over 8 days, with the hydrogel losing shape fidelity by day 9 and completely degrading by day 12. In agreement with the observed decrease in compressive moduli, the swelling ratios of $NorHA_{CA}$ hydrogels increased with time. For example, the swelling ratio of $NorHA_{CA}$ (5 wt.%, 40% mod.) hydrogels increased from 16.1 ± 2.8 to 46.3 ± 10.2 over the same 8-day period, likely due to an increase in the mesh size of the network as a result of degradation and reduced crosslinking. The morphology of hydrogels is relatively uniform in the swollen state during degradation (Figure S6). Interestingly, we note that the hydrolysis of $NorHA_{CA}$ is temperature dependent, which provides important insight towards storage of these hydrolytically degradable hydrogels (Figure S7). It is also important to note that the degradation of $NorHA_{CA}$ hydrogels in vivo would also be controlled by hyaluronidases, in addition to hydrolysis. Depending on the concentration of hyaluronidase, $NorHA_{CA}$ (5 wt.%, 40% mod.) hydrogels undergo complete degradation between 3 to 12 days (Figure S8). To avoid confounding effects of enzyme activity and hydrolysis, the present study is focused on understanding the hydrolytic stability of $NorHA_{CA}$ hydrogels, however, future studies are warranted to systematically study the role of hyaluronidase in degradation of $NorHA_{CA}$ hydrogels for specific applications.

3.2. Modeling and Tuning the Degradation of $NorHA_{CA}$ Hydrogels.

Several theoretical models have been previously developed to describe the bulk degradation of hydrogels crosslinked via free radical crosslinking,[32-34] step-growth crosslinking,[35,36] and mixed modes of crosslinking (i.e., concurrent radical and step-growth crosslinking).[37] However, many of the models that characterize the degradation of step-growth hydrogels involve hydrogels composed of small molecule monomers and/or multi-arm macromers with a fixed number of functional groups, resulting in relatively ideal network structures.[35] In contrast, the step-growth crosslinking of long $NorHA_{CA}$ macromers may exhibit a distribution of molecular weights or degrees of modification, which could result in random network architectures with variable mesh sizes throughout the hydrogel. Statistical-co-kinetic models have been previously developed and combined with Monte Carlo simulations to recapitulate the random and differential hydrolysis of crosslinks.[28] Moreover, the averaging of these random and discrete events at the microscale may provide insights into the network mesh size of the hydrogel over time. Building from this prior work, we develop a model that simulates the stochastic degradation of crosslinks in $NorHA_{CA}$ hydrogels to determine theoretical degradation rate constants (k) for investigated hydrogel formulations. Model simulations are iteratively performed across randomly generated network architectures to identify degradation rate constants that best corroborate experimental mass swelling ratios and compressive moduli (Figure 4). Generally, increasing the macromer concentration or the degree of modification used for $NorHA_{CA}$ hydrogel formation results in lower theoretical degradation rate constants (Table S2). While the model validates the observed degradation behavior of investigated $NorHA_{CA}$ hydrogels, as indicated by simulated mass swelling profiles (Figure S9), all of the investigated hydrogel formulations degrade within a few days to weeks. Differences in theoretical

and experimental degradation behavior exist and can be attributed to several simplifying assumptions (e.g., neglecting the molecular weight dispersity of macromers or the effect of changing carboxylic acid group density with degree of modification that can influence the rate of hydrolysis).

Longer degradation timescales are often desirable for applications such as tissue engineering scaffolds, where the rate of hydrogel degradation must be more selectively balanced with the rate of repair tissue formation.[38] To further tune and extend the degradation timescales of $NorHA_{CA}$ hydrogels, we next fabricate hydrogels from both degradable ($NorHA_{CA}$) and non-degradable (NorHA) macromers (Figure 5a). NorHA macromer is synthesized as previously described to modify the primary alcohols of HA with norbornene function groups.[21] Unlike $NorHA_{CA}$, the pendant norbornenes on NorHA lack an additional carboxylic acid group. As a result, hydrogels formed from solely NorHA macromer are much more stable in PBS at 37 °C, as evidenced by the minimal amount of uronic acid released (~3%) and the minimal amount of swelling observed after 28 days (Figure 5b, c). Although the compressive moduli of NorHA hydrogels (5 wt.%, 30% mod.) decrease from 152.3 ± 4.5 kPa to 104.1 ± 5.5 kPa over 28 days (Figure 5d), the reverse gelation typically seen with $NorHA_{CA}$ hydrogels (5 wt.%, 40% mod.) by day 12 was not observed.

With these two macromers available, we expect that combinations of $NorHA_{CA}$ with relatively small amounts of NorHA within the hydrogel would lower the overall hydrogel degradation rate through the formation of partially degradable (between hydrolytically labile and stable norbornenes) or completely non-degradable (between hydrolytically stable norbornenes) crosslinks. At a fixed total macromer concentration of 5 wt.%, increasing the amount of NorHA from 0 to 0.5 wt.% prolongs the degradation time by 6 days (Figure 5). The mass swelling ratio for $NorHA_{CA}$/NorHA hydrogels containing 0.5 wt.% NorHA macromer increases gradually from 15.6 ± 1.5 to 29.9 ± 2.5 over 8 days in comparison to the rapid increase from 16.1 ± 2.8 to 46.3 ± 10.2 for $NorHA_{CA}$ hydrogels without any NorHA macromer over the same time. Interestingly, further increasing the relative concentration of NorHA within $NorHA_{CA}$/NorHA hydrogels results in hydrogels that degrade slowly and do not undergo reverse gelation over at least 28 days. For instance, the compressive moduli of composite hydrogels ($NorHA_{CA}$ = 4 wt.%, NorHA = 1 wt.%) decreased from 84.1 ± 5.1 kPa to 3.6 ± 0.5 kPa over the first 21 days of incubation, but then remains fairly constant over the subsequent 7 days at an average modulus of 3.4 kPa; this may be attributed to the presence of purely non-degradable crosslinks within the composite network. Similar trends are also observed for the mass swelling ratio when the relative amount of NorHA macromer is increased within the hydrogel. Although these results show only modest changes in material properties at early times, the extension and control over degradation times through copolymers may prove quite useful depending on the application.

As a further examination of degradation, the subsequent increase in mesh size due to network degradation facilitates release of encapsulated proteins via diffusion to the surrounding medium. To investigate the effect of payload size, we quantify the cumulative release of bovine serum albumin (BSA, ~66 kDa) and polystyrene particles (0.2 μm), whereas to assess the effect of payload charge, we investigate the release of lysozyme (positively charged protein, ~14 kDa) from $NorHA_{CA}$ (5 wt.%, 40% mod.) hydrogels

(Figure S10). As expected, we conclude that the release of 0.2 μm particles is the slowest. However, despite being smaller in size than BSA, the release of lysozyme initially matches that of BSA but slows over time likely due to the electrostatic interactions between the protein and the negatively charged carboxyl groups on the norbornene moiety of $NorHA_{CA}$. Tuning the degradation time of $NorHA_{CA}$ with mixtures of non-degradable NorHA macromer can also be useful for altering release profiles of proteins (such as BSA) encapsulated within the hydrogel (Figure S10).

3.3. DLP-based 3D Printing of $NorHA_{CA}$ Hydrogels.

We extend the utility of our hydrolytically degradable $NorHA_{CA}$ resin to form 3D constructs via DLP-based 3D printing. DLP-based printing utilizes micromirror devices to project spatial light patterns onto a build stage, which moves vertically in a layer-by-layer manner, allowing for the fabrication of complex scaffolds.[39,40] The pattern fidelity and print resolution can be controlled with the use of light-attenuating additives (photoabsorbers such as tartrazine) that confine the polymerization to a desired layer thickness.[29] $NorHA_{CA}$ (5 wt.%, 40% mod.) is employed for DLP-based 3D printing studies due to its relatively longer degradation timeline of 12 days. Furthermore, the $NorHA_{CA}$ (5 wt.%, 40% mod.) precursor solution exhibits low viscosity (< 10 Pa s), making it suitable as a DLP resin (Figure S11). Working curves for the $NorHA_{CA}$ resin with different tartrazine concentrations are first obtained to identify an optimal gelation time for printing (Figure S12).[41] To this end, constructs could be printed with tartrazine (1 mM), exposure times of 6 s per layer, and a voxel step size of 100 μm. Post-printing, the constructs are washed and exposed to visible light to crosslink any remaining unreacted norbornenes (Figure 6a). Further, post-curing of 3D printed $NorHA_{CA}$ hydrogel discs results in an increase in compressive modulus by ~41.2 kPa (Figure S13). In addition, printability assessments of $NorHA_{CA}$ are performed to characterize the print resolution and shape fidelity of printed constructs over time (Figure S14). The lowest resolution of void space that can be reliably printed in an xy plane with $NorHA_{CA}$ resin is 500 μm. Although these hydrogels undergo swelling as a result of hydrolysis, they generally retain their printed shape with void spaces. The advantageous precision of DLP is clear from our ability to print intricate geometries such as knotted patterns, 3D gyroids, pyramids, 3D building blocks, and wheels (Figure 6b,c). In addition, we are able to print anatomically relevant shapes, such as a model femoral condyle. Next, we compare the degradation behavior of 3D printed $NorHA_{CA}$ hydrogel discs with those fabricated via simple casting into a mold (Figure 6d). Observed differences in the cumulative uronic acid release and compressive modulus over time can be attributed to the lower crosslink density achieved during DLP due to the use of photoabsorber and the low light exposure times used for the crosslinking of each print layer. Consistent with previous studies,[42] the use of photoabsorber creates a gradient in construct crosslinking density, causing a reduction in mechanical properties, as seen between the 3D printed and cast discs at day 0.

In addition to standard DLP printing, we leverage the maskless photolithography capability of the DLP printer towards 2D patterning of hydrogels. Thiol-ene step growth crosslinking can serve as a great platform to post-functionalize thiolated peptides or growth factors onto residual norbornene groups within preformed $NorHA_{CA}$ hydrogels, thereby

providing spatiotemporal tunability (Figure 6e). As a proof-of-concept, excess or unreacted norbornenes within bulk or 3D printed $NorHA_{CA}$ hydrogels can be soaked with thiolated fluorescent peptide (GCDDD-Fluor) and exposed to visible light on the DLP printer to generate spatial patterns (e.g., CU buffalo logo, checkerboard, and triangle) (Figure 6f). Given the short time (8 s) for post-functionalization and the use of 405 nm light, photopatterning of $NorHA_{CA}$ hydrogels can be promising for immobilization of therapeutic biomolecules toward designing 4D biomimetic models for tissue engineering in the future.

Next, we investigate cellular interactions with $NorHA_{CA}$ hydrogels in 2D as well as 3D. Bovine bone marrow derived mesenchymal stromal cells (bMSCs) are first seeded on bulk $NorHA_{CA}$ (5 wt.%, 40% mod.) hydrogels consisting of thiolated RGD (GCGYGRGDSPG, cell adhesive peptide, 2 mM). $NorHA_{CA}$ hydrogels support cell attachment and spreading as observed from the cell morphology over time (Figure 7a). Cell proliferation marked by an increase in cell number per unit area is observed over 7 days in culture (Figure 7b). Further, cell adhesive ligands can also be incorporated within the $NorHA_{CA}$ hydrogel during DLP printing (Figure 7c). Similar to cell colonization on bulk hydrogels, 3D printed macroporous scaffolds can be cellularized as visualized from the cell morphology at day 3 (Figure 7d). In addition to cell spreading, their viability upon encapsulation within $NorHA_{CA}$ hydrogels is also important for applications in tissue engineering. Cells can be successfully embedded in $NorHA_{CA}$ (5 wt.%, 40% mod.) hydrogels with > 85% cell viability over 7 days in culture (Figure 7e,f). Similarly, $NorHA_{CA}$ (5 wt.%, 15% mod.) hydrogels can also support high cell viability (> 88%) over time (Figure S15). This can be attributed to the ability of the $NorHA_{CA}$ hydrogels to undergo swelling and the subsequent reduction in compressive modulus over time that allows for enhanced nutrient transport and provides a dynamically soft microenvironment ideal for cell growth, respectively. The encapsulated cell density appears sparse over time due to the swelling and degradation of the hydrogel. Consequently, viability reduces from ~92% (day 1) to ~63% (day 7) for cells encapsulated within non-degradable NorHA (5 wt.%, 30% mod.) hydrogels (Figure S15). This is, in fact, expected given the high macromer concentration and high compressive modulus (~150 kPa) that remains fairly constant over the 7-day culture-period. We further demonstrate the capability for bioprinting cell-laden hydrogels formed with $NorHA_{CA}$ directly via DLP (Figure 7g). Using our $NorHA_{CA}$ bioresin containing bMSCs and cell-adhesive ligands, we 3D print high-fidelity hydrogels (e.g. discs, macroporous lattice) with embedded cells for potential applications towards tissue engineering (Figure 7h). 3D printed $NorHA_{CA}$ hydrogels are cytocompatible with ~80% viability three days post-printing (Figure S16). Lower cell viability in 3D bioprinted constructs as compared to bulk $NorHA_{CA}$ hydrogels can be a result of the higher photoinitiator concentrations and light intensities used in the DLP-printing process.

With the goal of designing scaffolds that are macroporous and suitable for tissue engineering applications, we 3D-printed proof-of-concept porous discs from $NorHA_{CA}$, $NorHA_{CA}$/NorHA composite (composed of 4.5 wt.% $NorHA_{CA}$ and 0.5 wt.% NorHA), and NorHA resin (Figure 8a). Similar to our bulk hydrogels, porous discs fabricated from $NorHA_{CA}$ and $NorHA_{CA}$/NorHA are seen to completely degrade by days 10 and 14, respectively, whereas those formed with NorHA are stable over the course of 28 days, with minimal release of uronic acid and minimal changes in the compressive modulus (Figure 8b). We next exploit

the rapid degradation of printed $NorHA_{CA}$ for the design of multi-material constructs, which allow for construct degradation to be spatially controlled towards the targeted release of therapeutic payloads. Non-degradable porous discs composed of NorHA are 3D printed and then in-filled with degradable $NorHA_{CA}$ hydrogel, which could be loaded with a cargo of interest (i.e., BSA; Figure 8c). As the $NorHA_{CA}$ hydrogel degraded, BSA was released from the interstitial spaces of the porous NorHA scaffold (Figure 8d). Importantly, multi-material designs such as this may be implemented for acellular tissue engineering scaffolds where (i) payloads such as growth factors are released to help recruit cells and (ii) void spaces allow for cell infiltration. As a proof-of-concept, we qualitatively demonstrate the evolution of pores upon degradation of $NorHA_{CA}$ resin (Figure 8c). This is quantitatively confirmed through the assessment of near total uronic acid release from the hydrogel by day 12. Furthermore, ~64% of bovine serum albumin (BSA, model protein) is released from the hydrogel within 1 day suggesting an initial burst, followed by a slower release thereafter (Figure 8d).

4. CONCLUSIONS

In summary, we utilize an aqueous carbic anhydride-based route for synthesis of norbornene-modified hyaluronic acid ($NorHA_{CA}$) with varying degrees of modification. The additional carboxylic group of $NorHA_{CA}$ enables the accelerated degradation of hydrogels formed via light-initiated thiol-ene crosslinking. The mechanical properties and degradation behavior of $NorHA_{CA}$ hydrogels can be readily modulated by changing the macromer concentration and/or the degree of modification, with the compressive modulus of hydrogels ranging from 1.5 to 150 kPa and degradation times between 3 to 14 days. The experimental trends observed in swelling of hydrogels are validated by a statistical-co-kinetic model that describes changes in network mesh size and macroscopic hydrogel properties as a function of crosslink hydrolysis. Importantly, the modeling approach employed is generalizable for other step-growth hydrogels composed of long macromer chains and may be adapted in future studies to predict degradation rate constants and hydrogel properties for alternative hydrogel formulations. Additional features may also be incorporated into the model to account for complex non-idealities such as intermolecular interactions between functional groups and diffusion limitations that arise with crosslinking. The degradation profile of $NorHA_{CA}$ hydrogels was further extended through the use of mixtures of degradable ($NorHA_{CA}$) and more stable (NorHA) macromers. Light-based rapid crosslinking of $NorHA_{CA}$ hydrogels allowed for processing into complex, macroporous structures with DLP-based 3D printing. 3D printed $NorHA_{CA}$ hydrogels are cytocompatible as seen from their ability to support cell attachment as well as high cell viability. Due to their tunability and predictable degradation behavior, $NorHA_{CA}$ hydrogels hold great promise as scaffolds for applications in biofabrication, tissue engineering and drug delivery.

Supplementary Material

Refer to Web version on PubMed Central for supplementary material.

ACKNOWLEDGMENT

This work was supported by the National Science Foundation (graduate research fellowship to J.H.G., Center for Engineering MechanoBiology CMMI: 15-48571) and the National Institutes of Health (R01AR077362, R01HL160616). The authors would like to thank Dr. Ghodsiehsadat Jahanmir and Dr. Ying Chau for helpful discussions on modeling the hydrolysis of $NorHA_{CA}$ hydrogels. The authors are grateful to Dr. Matthew Davidson, Dr. Claire Witherel and Nikolas Di Caprio for helpful discussions pertaining to hydrogel degradation. The authors would also like to thank the Anseth lab for use of their Zetasizer Nano as well as Dr. Chima Maduka and Bruce Kirkpatrick for assistance with measurements.

REFERENCES

(1). Zhang YS; Khademhosseini A Advances in Engineering Hydrogels. Science 2017, 356 (6337), eaaf3627. [PubMed: 28473537]

(2). Kharkar PM; Kiick KL; Kloxin AM Designing Degradable Hydrogels for Orthogonal Control of Cell Microenvironments. Chem. Soc. Rev 2013, 42 (17), 7335–7372. [PubMed: 23609001]

(3). Bhagat V; Becker ML Degradable Adhesives for Surgery and Tissue Engineering. Biomacromolecules 2017, 18 (10), 3009–3039. [PubMed: 28862846]

(4). Li J; Mooney DJ Designing Hydrogels for Controlled Drug Delivery. Nat. Rev. Mater 2016, 1 (12), 16071. [PubMed: 29657852]

(5). Boontheekul T; Kong HJ; Mooney DJ Controlling Alginate Gel Degradation Utilizing Partial Oxidation and Bimodal Molecular Weight Distribution. Biomaterials 2005, 26 (15), 2455–2465. [PubMed: 15585248]

(6). Kloxin AM; Kasko AM; Salinas CN; Anseth KS Photodegradable Hydrogels for Dynamic Tuning of Physical and Chemical Properties. Science 2009, 324 (5923), 59–63. [PubMed: 19342581]

(7). Yavitt FM; Brown TE; Hushka EA; Brown ME; Gjorevski N; Dempsey PJ; Lutolf MP; Anseth KS The Effect of Thiol Structure on Allyl Sulfide Photodegradable Hydrogels and Their Application as a Degradable Scaffold for Organoid Passaging. Adv. Mater 2020, 32 (30), 1905366.

(8). Stevens KR; Miller JS; Blakely BL; Chen CS; Bhatia SN Degradable Hydrogels Derived from PEG-Diacrylamide for Hepatic Tissue Engineering. J. Biomed. Mater. Res. Part A 2015, 103 (10), 3331–3338.

(9). Lueckgen A; Garske DS; Ellinghaus A; Mooney DJ; Duda GN; Cipitria A Enzymatically-Degradable Alginate Hydrogels Promote Cell Spreading and in Vivo Tissue Infiltration. Biomaterials 2019, 217, 119294. [PubMed: 31276949]

(10). Purcell BP; Lobb D; Charati MB; Dorsey SM; Wade RJ; Zellars KN; Doviak H; Pettaway S; Logdon CB; Shuman JA; Freels PD; Gorman JH; Gorman RC; Spinale FG; Burdick JA Injectable and Bioresponsive Hydrogels for On-Demand Matrix Metalloproteinase Inhibition. Nat. Mater 2014, 13 (6), 653–661. [PubMed: 24681647]

(11). Sridhar BV; Brock JL; Silver JS; Leight JL; Randolph MA; Anseth KS Development of a Cellularly Degradable PEG Hydrogel to Promote Articular Cartilage Extracellular Matrix Deposition. Adv. Healthc. Mater 2015, 4 (5), 702–713. [PubMed: 25607633]

(12). Huang J; Jiang X Injectable and Degradable PH-Responsive Hydrogels via Spontaneous Amino-Yne Click Reaction. ACS Appl. Mater. Interfaces 2018, 10 (1), 361–370. [PubMed: 29235844]

(13). Hu J; Chen Y; Li Y; Zhou Z; Cheng Y A Thermo-Degradable Hydrogel with Light-Tunable Degradation and Drug Release. Biomaterials 2017, 112, 133–140. [PubMed: 27760397]

(14). Wang Y; Zhang S; Benoit DSW Degradable Poly(Ethylene Glycol) (PEG)-Based Hydrogels for Spatiotemporal Control of SiRNA/Nanoparticle Delivery. J. Control. Release 2018, 287, 58–66. [PubMed: 30077736]

(15). Neumann AJ; Quinn T; Bryant SJ Nondestructive Evaluation of a New Hydrolytically Degradable and Photo-Clickable PEG Hydrogel for Cartilage Tissue Engineering. Acta Biomater. 2016, 39, 1–11. [PubMed: 27180026]

(16). Lin FY; Lin CC Facile Synthesis of Rapidly Degrading PEG-Based Thiol-Norbornene Hydrogels. ACS Macro Lett. 2021, 10 (3), 341–345. [PubMed: 35549061]

(17). Muir VG; Burdick JA Chemically Modified Biopolymers for the Formation of Biomedical Hydrogels. Chem. Rev 2021, 121 (18), 10908–10949. [PubMed: 33356174]

(18). Burdick JA; Prestwich GD; Burdick A; Prestwich GD Hyaluronic Acid Hydrogels for Biomedical Applications. Adv. Mater 2011, 23 (12), H41–H56. [PubMed: 21394792]

(19). Sahoo S; Chung C; Khetan S; Burdick JA Hydrolytically Degradable Hyaluronic Acid Hydrogels with Controlled Temporal Structures. Biomacromolecules 2008, 9 (4), 1088–1092. [PubMed: 18324776]

(20). Chung C; Beecham M; Mauck RL; Burdick JA The Influence of Degradation Characteristics of Hyaluronic Acid Hydrogels on in Vitro Neocartilage Formation by Mesenchymal Stem Cells. Biomaterials 2009, 30 (26), 4287–4296. [PubMed: 19464053]

(21). Gramlich WM; Kim IL; Burdick JA Synthesis and Orthogonal Photopatterning of Hyaluronic Acid Hydrogels with Thiol-Norbornene Chemistry. Biomaterials 2013, 34 (38), 9803–9811. [PubMed: 24060422]

(22). Münoz Z; Shih H; Lin CC Gelatin Hydrogels Formed by Orthogonal Thiol-Norbornene Photochemistry for Cell Encapsulation. Biomater. Sci 2014, 2 (8), 1063–1072. [PubMed: 32482001]

(23). McOscar TVC; Gramlich WM Hydrogels from Norbornene-Functionalized Carboxymethyl Cellulose Using a UV-Initiated Thiol-Ene Click Reaction. Cellulose 2018, 25 (11), 6531–6545.

(24). Guo K; Wang H; Li S; Zhang H; Li S; Zhu H; Yang Z; Zhang L; Chang P; Zheng X Collagen-Based Thiol-Norbornene Photoclick Bio-Ink with Excellent Bioactivity and Printability. ACS Appl. Mater. Interfaces 2021, 13 (6), 7037–7050. [PubMed: 33517661]

(25). Xiao X; Huang Z; Jiang X; Yang Y; Yang L; Yang S; Niu C; Xu Y; Feng L Facile Synthesize of Norbornene-Hyaluronic Acid to Form Hydrogel via Thiol-Norbornene Reaction for Biomedical Application. Polymer 2022, 245, 124696.

(26). Cesaretti M; Luppi E; Maccari F; Volpi N A 96-Well Assay for Uronic Acid Carbazole Reaction. Carbohydr. Polym 2003, 54 (1), 59–61.

(27). Burdick JA; Chung C; Jia X; Randolph MA; Langer R Controlled Degradation and Mechanical Behavior of Photopolymerized Hyaluronic Acid Networks. Biomacromolecules 2005, 6 (1), 386–391. [PubMed: 15638543]

(28). Jahanmir G; Abdekhodaie MJ; Chau Y Stochastic Modeling of Degradation Behavior of Hydrogels. Macromolecules 2018, 51 (11), 3941–3952.

(29). Grigoryan B; Paulsen SJ; Corbett DC; Sazer DW; Fortin CL; Zaita AJ; Greenfield PT; Calafat NJ; Gounley JP; Ta AH; Johansson F; Randles A; Rosenkrantz JE; Louis-Rosenberg JD; Galie PA; Stevens KR; Miller JS Multivascular Networks and Functional Intravascular Topologies within Biocompatible Hydrogels. Science 2019, 364 (6439), 458–464. [PubMed: 31048486]

(30). Dhand AP; Davidson MD; Galarraga JH; Qazi TH; Locke RC; Mauck RL; Burdick JA Simultaneous One-Pot Interpenetrating Network Formation to Expand 3D Processing Capabilities. Adv. Mater 2022, 34 (28), 2202261.

(31). Dimmitt NH; Arkenberg MR; De Lima Perini MM; Li J; Lin CC Hydrolytically Degradable PEG-Based Inverse Electron Demand Diels-Alder Click Hydrogels. ACS Biomater. Sci. Eng 2022, 8 (10), 4262–4273. [PubMed: 36074814]

(32). Metters AT; Anseth KS; Bowman CN A Statistical Kinetic Model for the Bulk Degradation of PLA-b-PEG-b-PLA Hydrogel Networks: Incorporating Network Non-Idealities. J. Phys. Chem. B 2001, 105 (34), 8069–8076.

(33). Leach JB; Bivens KA; Patrick CW; Schmidt CE Photocrosslinked Hyaluronic Acid Hydrogels: Natural, Biodegradable Tissue Engineering Scaffolds. Biotechnol. Bioeng 2003, 82 (5), 578–589. [PubMed: 12652481]

(34). Martens P; Metters AT; Anseth KS; Bowman CN A Generalized Bulk-Degradation Model for Hydrogel Networks Formed from Multivinyl Cross-Linking Molecules. J. Phys. Chem. B 2001, 105 (22), 5131–5138.

(35). Shih H; Lin CC Cross-Linking and Degradation of Step-Growth Hydrogels Formed by Thiol-Ene Photoclick Chemistry. Biomacromolecules 2012, 13 (7), 2003–2012. [PubMed: 22708824]

(36). Metters A; Hubbell J Network Formation and Degradation Behavior of Hydrogels Formed by Michael-Type Addition Reactions. Biomacromolecules 2005, 6 (1), 290–301. [PubMed: 15638532]

(37). Reddy SK; Anseth KS; Bowman CN Modeling of Network Degradation in Mixed Step-Chain Growth Polymerizations. Polymer 2005, 46 (12), 4212–4222.

(38). Zhao W; Jin X; Cong Y; Liu Y; Fu J Degradable Natural Polymer Hydrogels for Articular Cartilage Tissue Engineering. J. Chem. Technol. Biotechnol 2013, 88 (3), 327–339.

(39). Chartrain NA; Williams CB; Whittington AR A Review on Fabricating Tissue Scaffolds Using Vat Photopolymerization. Acta Biomater. 2018, 74, 90–111. [PubMed: 29753139]

(40). Lee M; Rizzo R; Surman F; Zenobi-Wong M Guiding Lights: Tissue Bioprinting Using Photoactivated Materials. Chem. Rev 2020, 120 (19), 10950–11027. [PubMed: 32662642]

(41). Lim KS; Levato R; Costa PF; Castilho MD; Alcala-Orozco CR; Van Dorenmalen KMA; Melchels FPW; Gawlitta D; Hooper GJ; Malda J; Woodfield TBF Bio-Resin for High Resolution Lithography-Based Biofabrication of Complex Cell-Laden Constructs. Biofabrication 2018, 10 (3), 034101. [PubMed: 29693552]

(42). Uzcategui AC; Muralidharan A; Ferguson VL; Bryant SJ; McLeod RR Understanding and Improving Mechanical Properties in 3D Printed Parts Using a Dual-Cure Acrylate-Based Resin for Stereolithography. Adv. Eng. Mater 2018, 20 (12), 1800876. [PubMed: 30766445]

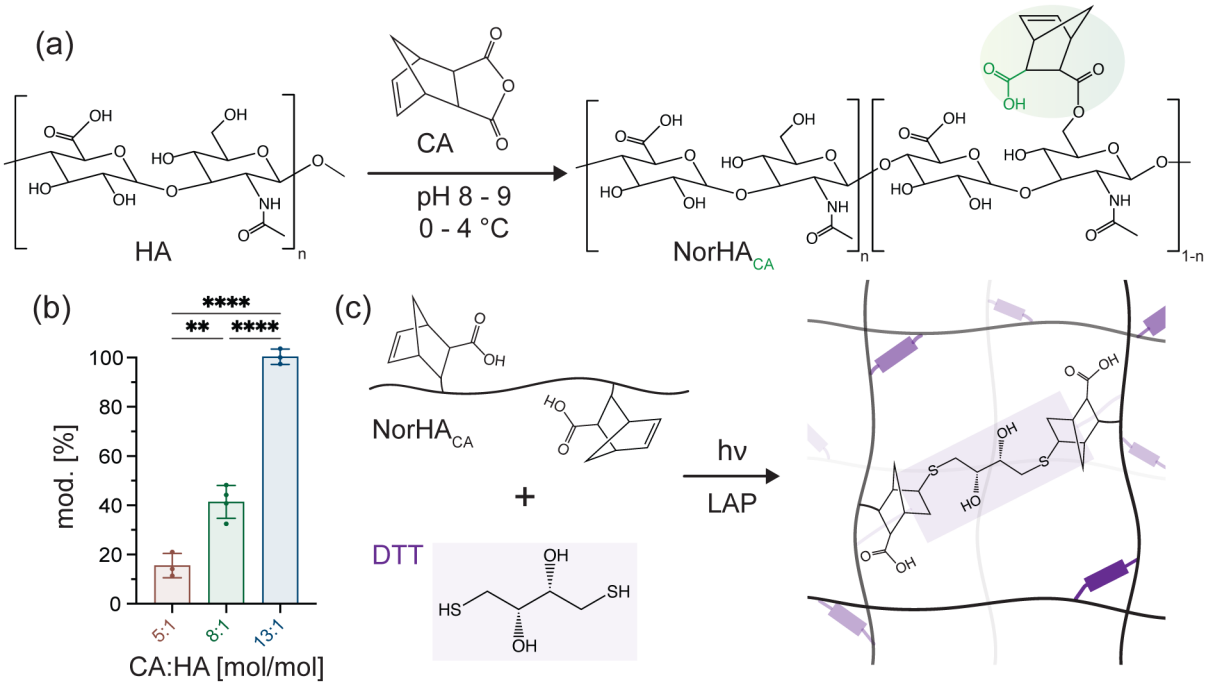

Figure 1.

Synthesis of NorHA$_{CA}$ macromer and hydrogels. (a) Reaction scheme for modification of sodium hyaluronate (HA) with cis-5-norbornene-endo-2,3-dicarboxylic anhydride (CA) to form norbornene-modified HA (NorHA$_{CA}$) (b) The degree of modification of HA with norbornene is tuned by changing the molar ration of CA to HA repeat units. Data are reported as mean ± SD; n ≥ 3; **p < 0.01; ****p < 0.0001 (c) Schematic representation of network formation by visible light induced thiol-ene step growth reaction between NorHA$_{CA}$ and dithiothreitol (DTT) in the presence of photoinitiator (lithium phenyl-2,4,6-trimethylbenzoylphosphinate, LAP).

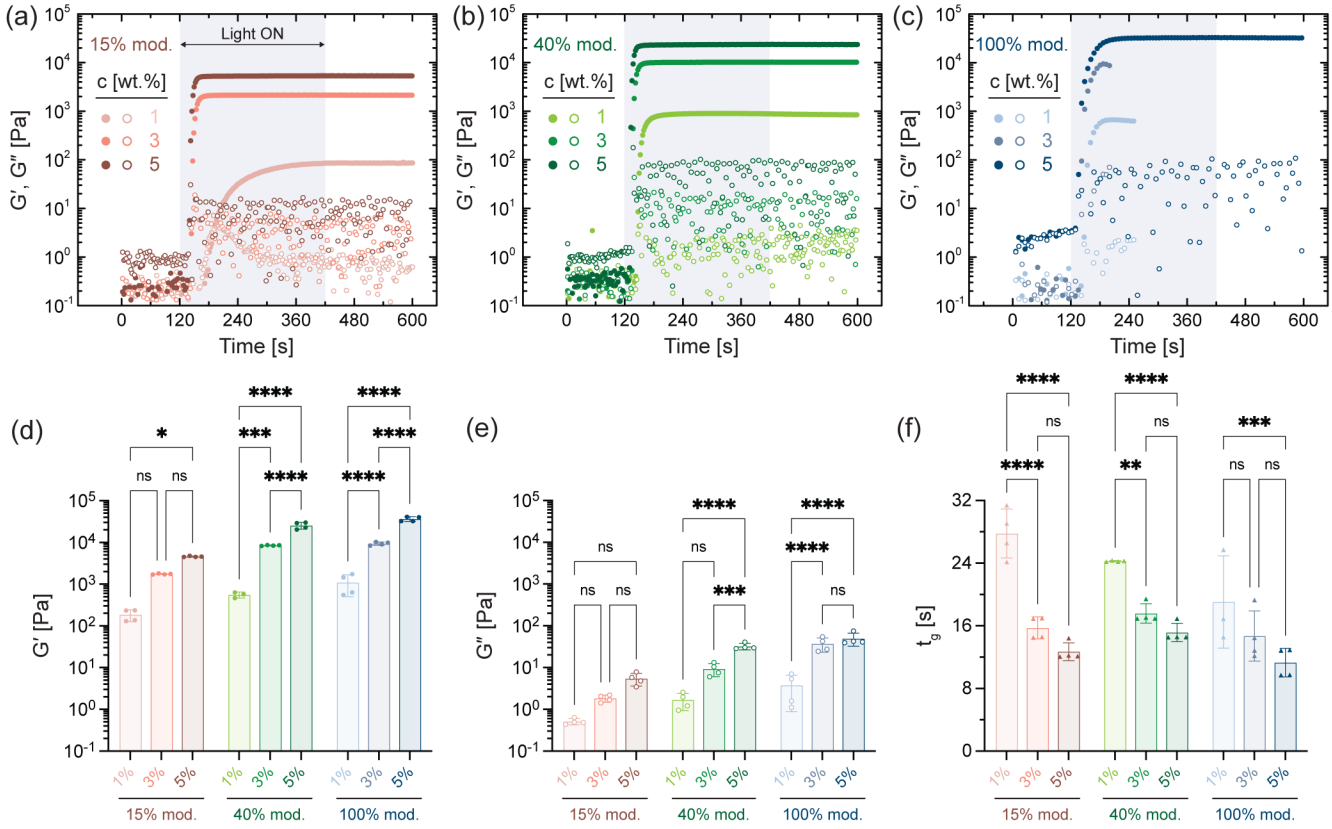

Figure 2.

Rheological characterization of NorHA$_{CA}$ hydrogels. Storage modulus, G′ (closed symbol) and loss modulus, G″ (open symbol) as a function of time for NorHA$_{CA}$ formulations with varying macromer concentrations (1, 3, 5 wt.%) and degrees of modification: (a) 15% mod., (b) 40% mod., (c) 100% mod. Shaded box indicates the time period between 120 and 420 seconds for which visible light is introduced. Note that 1 and 3 wt.% of the 100% mod. are not testable past reaching the plateau, as samples likely separate from the plates. (d) G′, (e) G″, and (f) time to gel point (t_g) for various NorHA$_{CA}$ hydrogel formulations investigated. Statistical comparisons of all groups within each degree of modification shown on graphs. Data are reported as mean ± SD; n ≥ 3; ns = not significant; *p < 0.05; **p < 0.01; ***p < 0.001; ****p < 0.0001.

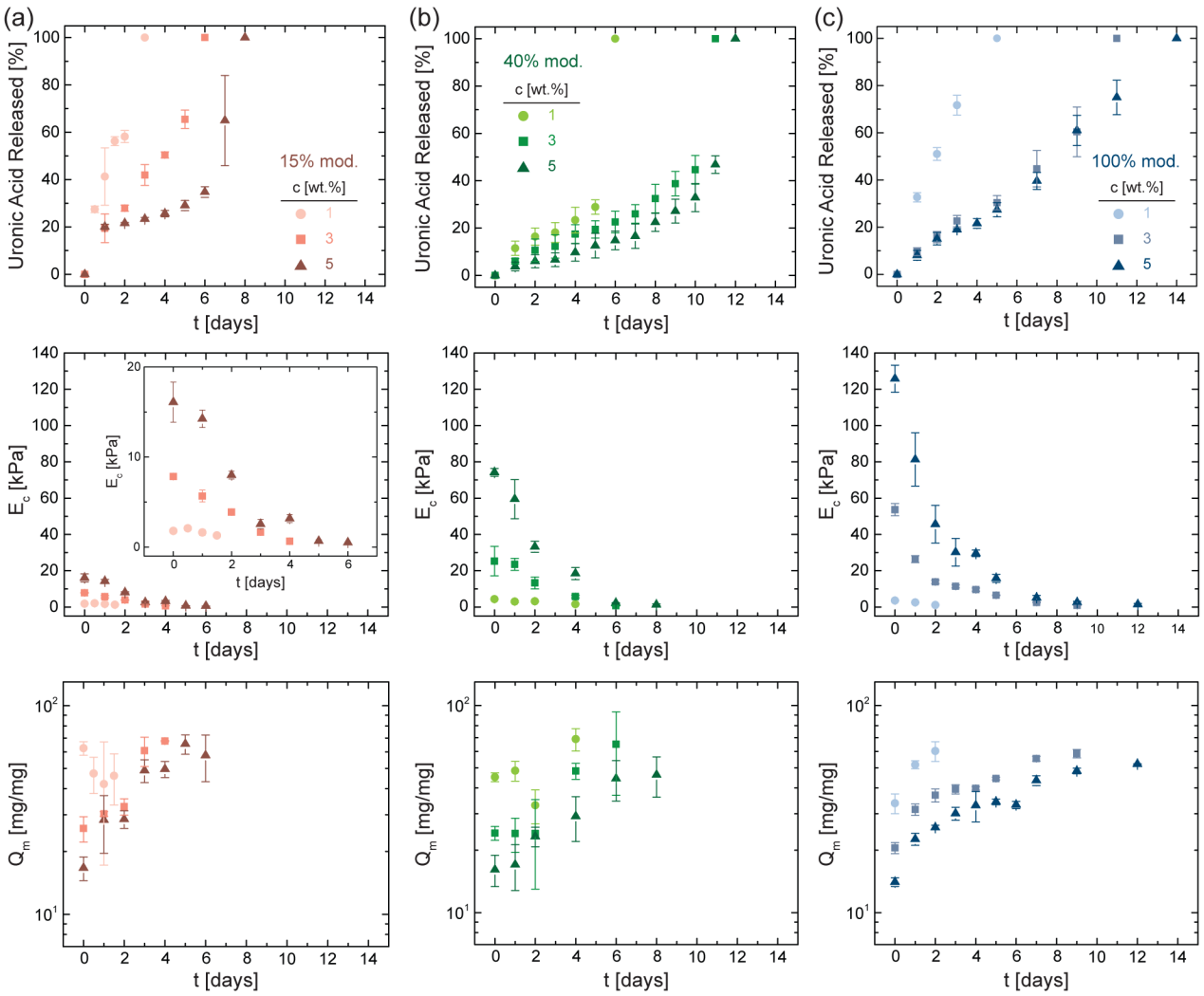

Figure 3.

Characterization of $NorHA_{CA}$ hydrogel degradation. Cumulative uronic acid released, compressive modulus (E_C), and mass swelling ratio (Q_m) over time (t) for varying $NorHA_{CA}$ macromer concentrations (1, 3, 5 wt.%) and degrees of modification: (a) 15% mod., (b) 40% mod., and (c) 100% mod. Data are reported as mean ± SD; n ≥ 3.

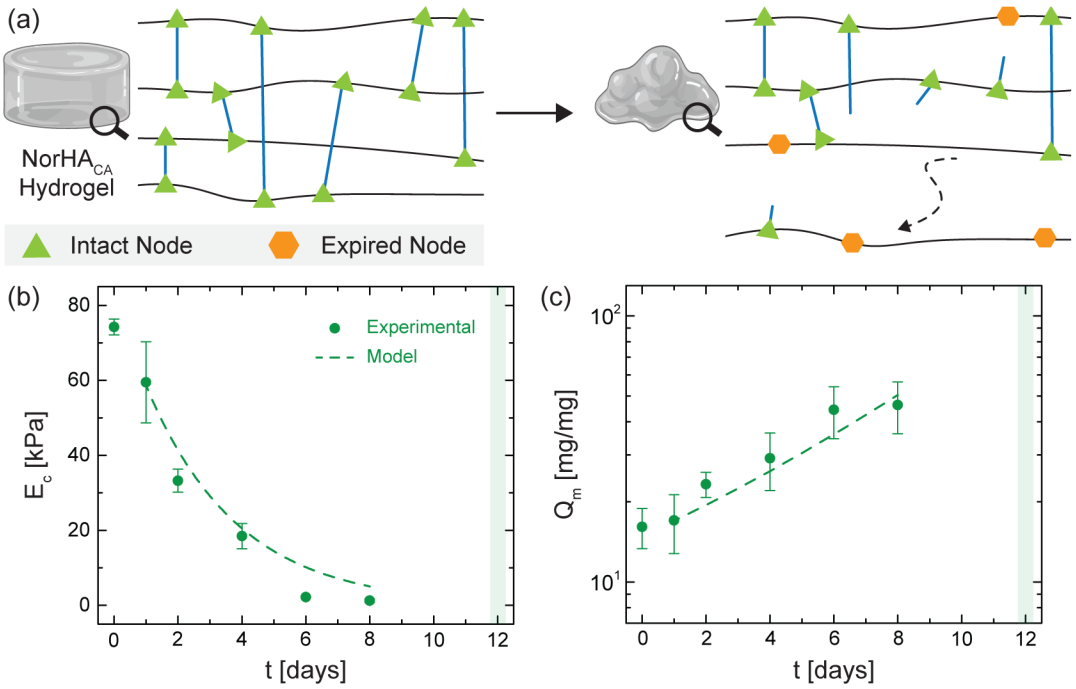

Figure 4.

Modeling the degradation behavior of NorHA$_{CA}$ hydrogels. a) Schematic overview of the modeling approach employed to characterize NorHA$_{CA}$ hydrogel degradation. Model fit (dotted line, $k = 0.350$ day^{-1}) for the (b) compressive modulus (E_C) and (c) mass swelling ratio (Q_m) of a select NorHA$_{CA}$ hydrogel (5 wt.%, 40% mod.) over time, with comparisons to experimental data (symbols). Shaded box indicates time point for complete degradation of the hydrogel. Data are reported as mean ± SD; n ≥ 3. Hydrogel schematics created using BioRender.

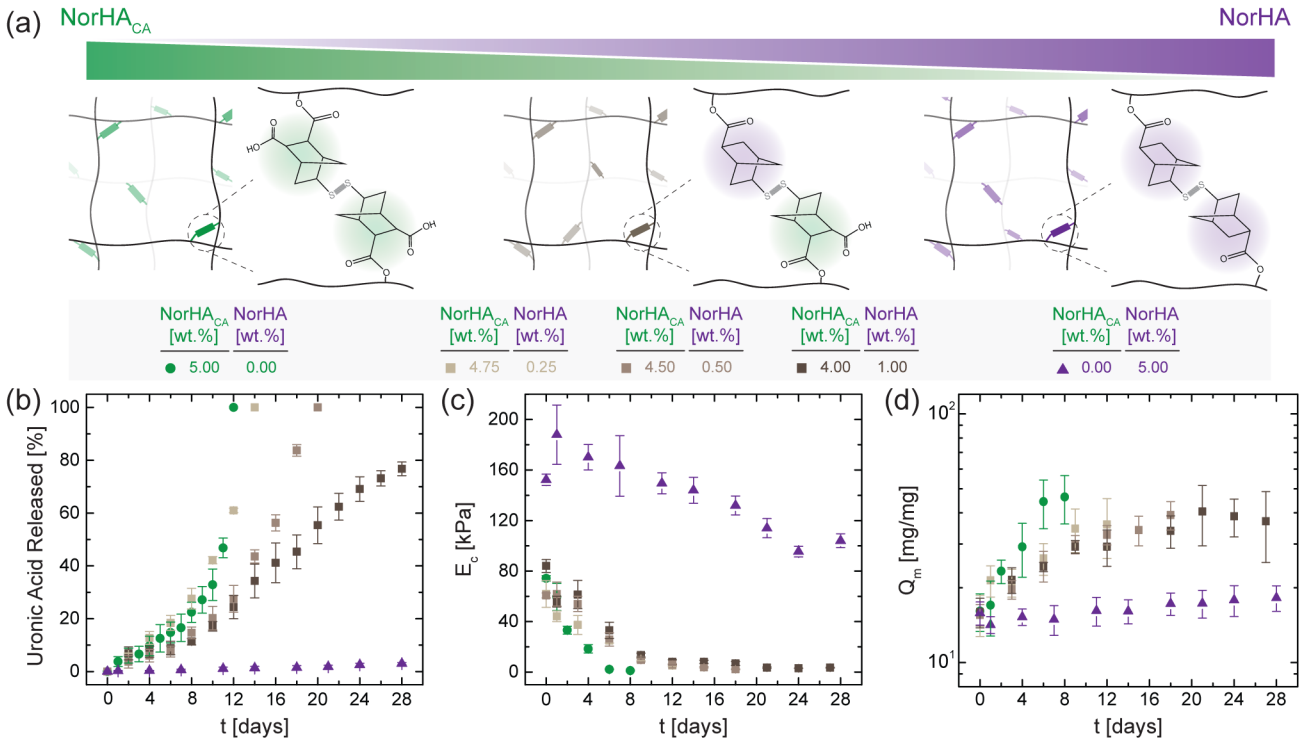

Figure 5.

Tuning hydrogel degradation behavior by combining degradable and non-degradable macromers. (a) Schematic illustration of networks composed of $NorHA_{CA}$ alone, NorHA alone, and $NorHA_{CA}$/NorHA mixtures (4.75:0.25, 4.50:0.50, 4.00:1.00). (b) Cumulative uronic acid released, (c) compressive modulus (E_C), and (d) mass swelling ratio (Q_m) over time (t) for hydrogels formed with $NorHA_{CA}$, NorHA, and $NorHA_{CA}$/NorHA mixtures. The total macromer concentration was kept fixed at 5 wt.%. Data are reported as mean ± SD; n ≥ 3.

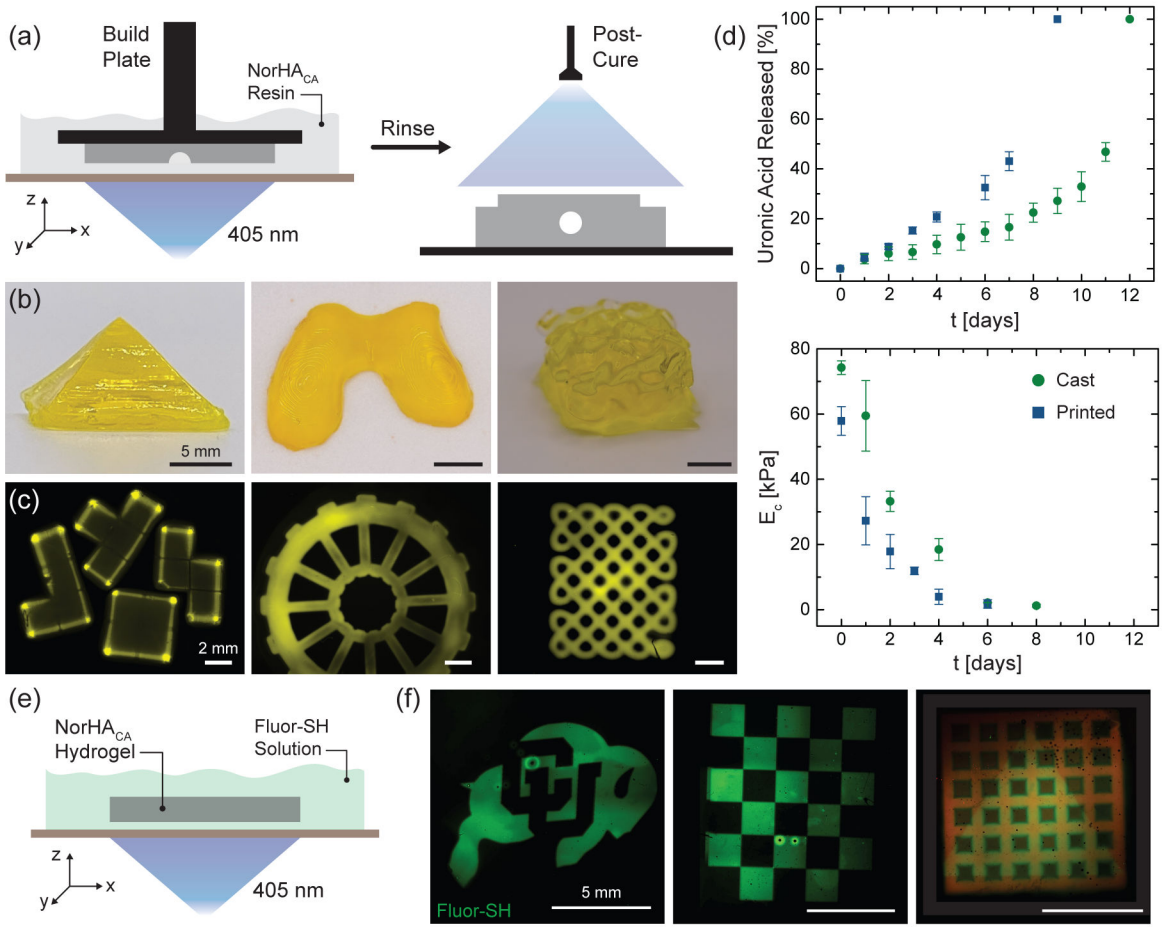

Figure 6.

3D printing and patterning of NorHA$_{CA}$ hydrogels. (a) Schematic illustration of digital light processing (DLP)-based fabrication of NorHA$_{CA}$ hydrogels (5 wt.%, 40% mod.) and post-print curing to improve mechanical properties. (b) Photographs of pyramid, femoral condyle, and 3D gyroid (in air). Scale bar: 5 mm. (c) Fluorescence images of 3D building blocks, wheel, and knotted pattern printed with NorHA$_{CA}$ resin. Scale bar: 2 mm. (d) Comparison of uronic acid release and compressive modulus (E_C) over time (t) for casted and 3D printed NorHA$_{CA}$ hydrogels. (e) Schematic illustration of maskless photo-patterning of NorHA$_{CA}$ hydrogels (5 wt.%, 40% mod.) with fluorescent thiol (GCDDD-Fluor) on the DLP-printer. (f) Fluorescence maximum projection image of 2D patterned CU buffalo, checkerboard, triangle on NorHA$_{CA}$ bulk hydrogel and printed macroporous lattice (shown in red), respectively. Scale bar: 5 mm.

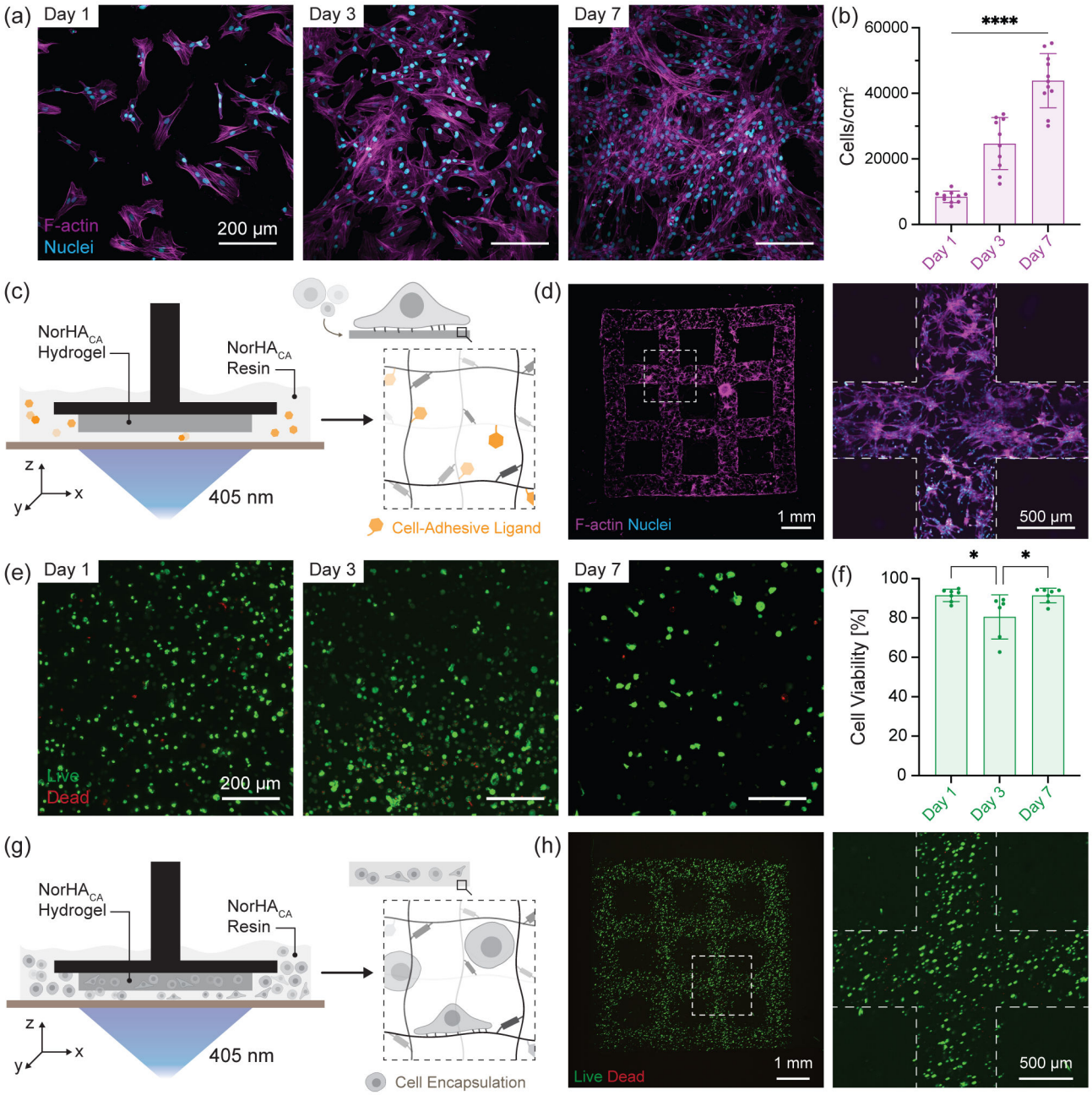

Figure 7.

Cell interactions with NorHA$_{CA}$ hydrogels. (a) Representative fluorescence micrographs of bovine bone marrow derived mesenchymal stromal cells (bMSCs) seeded on NorHA$_{CA}$ hydrogels (5 wt.%, 40% mod.) over time (1,3,7 days). F-actin (magenta) and nuclei (cyan). Scale bar: 200 µm. (b) Quantification of the number of cells per unit area over time. Data are reported as mean ± SD; n ≥ 3; ****p < 0.0001 (c) Schematic illustration of digital light processing (DLP)-based fabrication of NorHA$_{CA}$ hydrogels with cell adhesive peptides (GCGYGRGDSPG, 2 mM) and post-seeded with cells. (d) Representative maximum projection image of bMSCs seeded on a NorHA$_{CA}$ macroporous lattice at day 3. F-actin (magenta) and nuclei (cyan). Scale bars: 1 mm and 500 µm. Dotted line indicates lattice

boundary. (e) Representative fluorescence micrographs of bMSCs encapsulated in $NorHA_{CA}$ (5 wt.%, 40% mod.) bulk hydrogels over time (1,3,7 days). Live (calcein AM, green), Dead (ethidium homodimer-1, red). Scale bar: 200 μm. (f) Percentage of viable (live) cells over time in $NorHA_{CA}$ hydrogels. Data are reported as mean ± SD; $n \geq 3$; $^*p < 0.05$ (g) Schematic representation of DLP-based 3D printing of $NorHA_{CA}$ hydrogels (5 wt.%, 40% mod.) with bMSCs. (h) Representative maximum projection image of bMSCs encapsulated in $NorHA_{CA}$ macroporous lattice at day 1. Live (calcein AM, green), Dead (ethidium homodimer-1, red). Scale bars: 1 mm and 500 μm. Dotted line indicates lattice boundary.

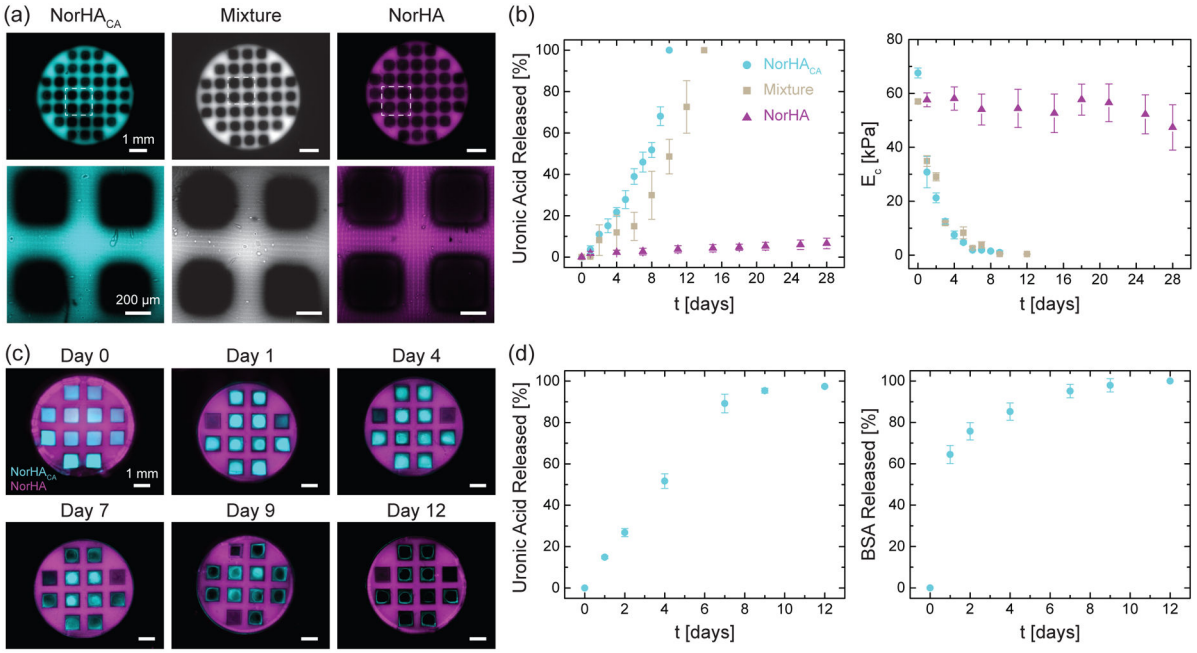

Figure 8.

Fabrication of macroporous constructs from degradable NorHA$_{CA}$, non-degradable NorHA, and NorHA$_{CA}$/NorHA mixtures. (a) (top) Fluorescence images of 3D printed macroporous discs. Scale bar: 1 mm. (bottom) Representative maximum projection images of the pores within the discs. Scale bar: 200 μm. (b) Cumulative uronic acid release and compressive modulus (E_C) over time (t) for 3D printed macroporous NorHA$_{CA}$, NorHA, and NorHA$_{CA}$/NorHA discs. The total macromer concentration was kept fixed at 5 wt.% and the NorHA$_{CA}$/NorHA mixture consists of 4.5 wt.% NorHA$_{CA}$ and 0.5 wt.% NorHA. (c) Fluorescence images of macroporous NorHA discs (magenta) filled with NorHA$_{CA}$ (cyan) over the course of degradation. Scale bar: 1 mm. (d) Cumulative uronic acid and encapsulated bovine serum albumin (BSA) release from filled NorHA$_{CA}$ hydrogels over time (t).